Turkish Journal of Electrical Engineering and Computer Sciences

Volume 23 | Number 6 Article 32

1-1-2015

Performance analysis of a low-cost current-source 1-ph grid-connected PV inverter

GÜRHAN ERTAŞGIN

WEN LIANG SOONG

NESIMI ERTUGRUL

Recommended Citation

ERTAŞGIN, GÜRHAN; SOONG, WEN LIANG; and ERTUGRUL, NESIMI (2015) "Performance analysis of a low-cost current-source 1-ph grid-connected PV inverter," *Turkish Journal of Electrical Engineering and Computer Sciences*: Vol. 23: No. 6, Article 32. https://doi.org/10.3906/elk-1404-294

Available at: https://journals.tubitak.gov.tr/elektrik/vol23/iss6/32

Turkish Journal of Electrical Engineering & Computer Sciences

http://journals.tubitak.gov.tr/elektrik/

Research Article

Turk J Elec Eng & Comp Sci
(2015) 23: 1981 – 1995
© TÜBİTAK
doi:10.3906/elk-1404-294

Performance analysis of a low-cost current-source 1-ph grid-connected PV inverter

Gürhan ERTAŞGIN[1,*], **Wen Liang SOONG**[2], **Nesimi ERTUGRUL**[2]
[1]School of Electrical and Electronic Engineering, Bilecik Şeyh Edebali University, Bilecik, Turkey
[2]School of Electrical and Electronic Engineering, University of Adelaide, North Terrace, Adelaide, Australia

Received: 15.04.2014 • **Accepted/Published Online:** 14.07.2015 • **Printed:** 30.11.2015

Abstract: This paper investigates the design and performance of a 150 W single-phase current-source grid-connected inverter topology that is based on a PV array and DC link inductor acting as a constant-current source. The inverter is implemented using a single boost switch, an H-bridge inverter, and a CL output filter. The inverter output current is simply controlled using the boost switch and open-loop or feedforward control. The dark I-V configuration is used to simulate two series PV modules. Comprehensive test results are obtained to validate the computer simulation results. Furthermore, the proposed inverter's ability to deliver a sinusoidal current to the grid while meeting the appropriate standards, i.e. total harmonic distortion and power factor requirements, is also examined for various modulation index values and irradiances.

Key words: Photovoltaic cells, pulse width modulation inverters, solar power generation, switching converters

1. Introduction

Limited fossil fuel resources, high demands for electrical energy, and concerns about pollution have prompted research into renewable energy sources. Developments in the production of photovoltaic (PV) cells have made these more cost-effective. It is convenient to feed the power generated by PV cells back into the power grid using a grid-connected inverter (GCI). Research into GCIs for PV applications is focused on reducing costs and improving performance and reliability while meeting the grid standards.

Early GCIs were of the current-source type, which used a DC link inductor to create a constant-current source and line-frequency commutated switches to produce a square-wave output current. Despite its simplicity, the output current needed significant filtering to meet the grid THD standards [1]. Some interest has been reported in the use of PWM controlled current-source inverters (CSIs) [2–6]. A gate turn-off thyristor (GTO)-based H-bridge grid-connected CSI has been proposed, which used PWM control. Although the switching losses of GTOs are relatively high [7], they can block reverse voltage and hence eliminate the need for a series diode. However, due to the limited switching speeds of GTOs, this approach has been used mainly at higher output powers. As expected, the input DC link inductor losses in this topology were found to result in a substantial reduction in the inverter efficiency. Another topology in the literature is a line-commutated soft-switched CSI consisting of IGBTs and diodes as a resonant switch and H-bridge inverter. This concept produced a soft-switched CSI and improved efficiency. However, the inverter control is more complicated and the number of components is increased. This increases the inverter cost while reducing reliability. Although some recent single-

---

[*] Correspondence: gurhan@ieee.org

phase current-source PV topologies [8–14] have better efficiency and THD performances, they have additional circuitry, including passive and switching components in the main current path to reduce the DC link inductor size. The increased number of components and more complex control could cause extra losses and reliability issues.

Previously, some work was performed by the authors on a switched-mode rectifier (SMR)-based novel topology and H-bridge inverter [15–18]. This topology is an extension of an SMR circuit that was proposed for automotive applications [19], where it is used as a DC-DC converter. Some modifications were done associated with the SMR concept to use this topology as a GCI for wind turbines and PV arrays. It was implemented employing open-loop control to create PWM signals with only one high-frequency switch. A large DC link inductor is used to supply a constant-current source and to smooth the instantaneous power fluctuations from the inverter side at twice the grid frequency (in this case, 100 Hz). The proposed inverter is an improved design of the inverter discussed in [16], including improved circuit layout for reliability, optimized DC link inductor to reduce losses, and an optimized low-pass filter to meet the grid harmonic and power factor (PF) standards.

1.1. Proposed topology of the photovoltaic inverter

The proposed GCI is based on a constant current-source. This is achieved using a PV array with a DC link inductor. Figure 1 shows a block diagram of the proposed inverter, along with the expected input and output currents of the four inverter stages, i.e. the constant-current source, waveshaper (WS), unfolding circuit (UC), and low-pass filter. The inverter operates from an essentially constant input current, delivered by the PV modules through the DC link inductor. The current waveshaper and unfolding circuit stages are used to produce a unipolar PWM current, which is filtered and fed to the grid, via the low-pass filter to produce a sinusoidal output current.

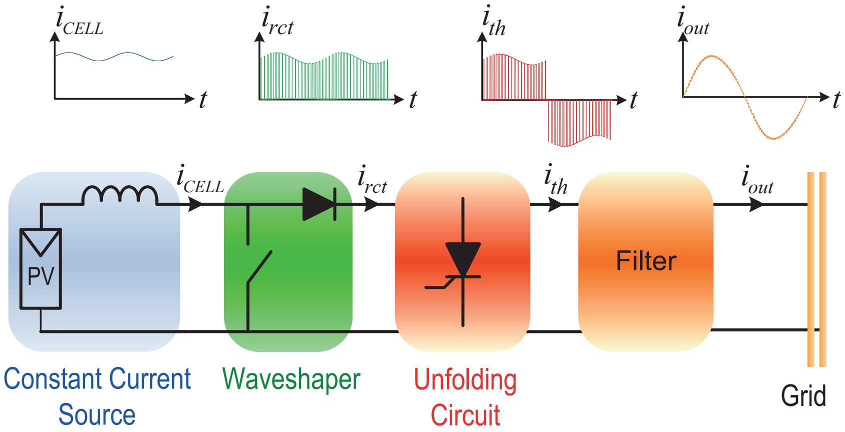

Figure 1. Proposed grid-connected CSI topology for PV applications showing constant-current input, and the current waveforms for each stage.

1.2. PV array

The PV modules used in this application are the BP380U model from BP Solar. The PV array output is simulated with an experimental technique called the “dark I-V test”, which was used to simulate sunlight operation of the PV cells. The measurement technique is also commonly used to investigate the performance specifications of solar modules [20]. The dark I-V test circuit is given in Figure 2a and the block diagram when connected to the CSI is shown in Figure 2b. The constant-current source of the dark I-V arrangement is set to the short-circuit current (I_{SC}) value, which corresponds to 1 kW/m^2 irradiance value. It involves covering the PV module (to eliminate the light-induced current) and using a constant-current source to simulate the light-induced current. This is convenient as the testing can be performed indoors and the irradiance level can be easily controlled and kept constant during the test. However, the temperature of the PV modules may not be realistic as PV models often operate at much hotter temperatures than 25 °C, except in cold climates.

Simulated and tested current versus voltage and power versus voltage loci can be seen in Figures 2c and 2d. The simulations are shown for irradiances of G = 0.25–1 kW/m^2 at 10 °C, while the measured results correspond to 1 kW/m^2 at a module temperature of 10 °C. The good agreement supports the use of the dark I-V method.

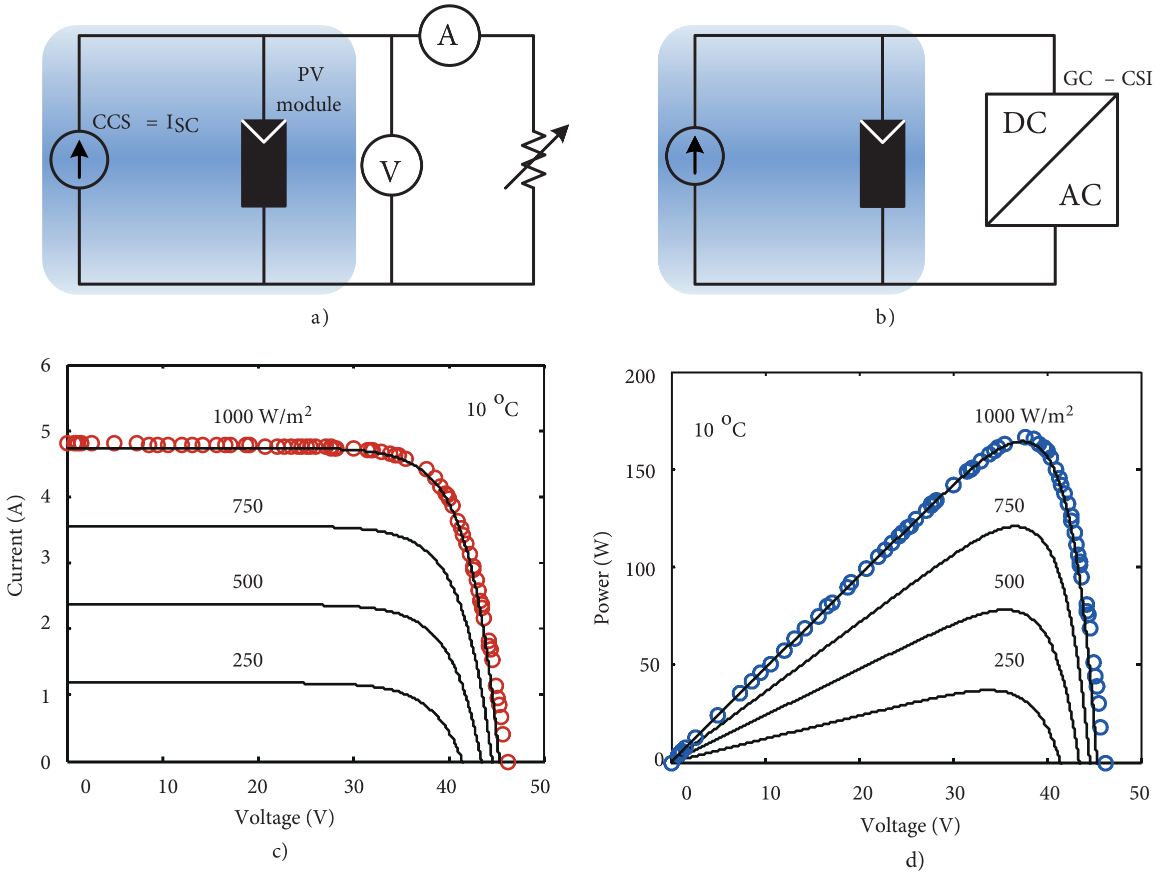

Figure 2. a) Dark I-V test arrangement block diagram, b) dark I-V implementation block diagram with grid-connected CSI, and c) current-voltage and d) power-voltage loci for the PV modules at various irradiance values. The solid lines represent calculations and the symbols represent dark I-V measurement results.

2. CSI implementation

2.1. MPPT algorithm

The PV inverters are controlled to extract maximum power from the PV arrays using a maximum power point tracking (MPPT) algorithm. The output power of the CSI can be controlled using open-loop or closed-loop control. Since the PV module current-voltage characteristics will vary according to operating conditions, so too will the current corresponding to the MPPT. The inverter must be able to vary the solar array output current to maximize the output power. This is done by changing the modulation index (m_A), which changes the amplitude of the sinusoidal duty-cycle modulation applied to the waveshaper in Figure 1. The implemented MPPT algorithm is based on maximizing the inverter output current using the perturb-and-observe method [2], as seen in Figure 3.

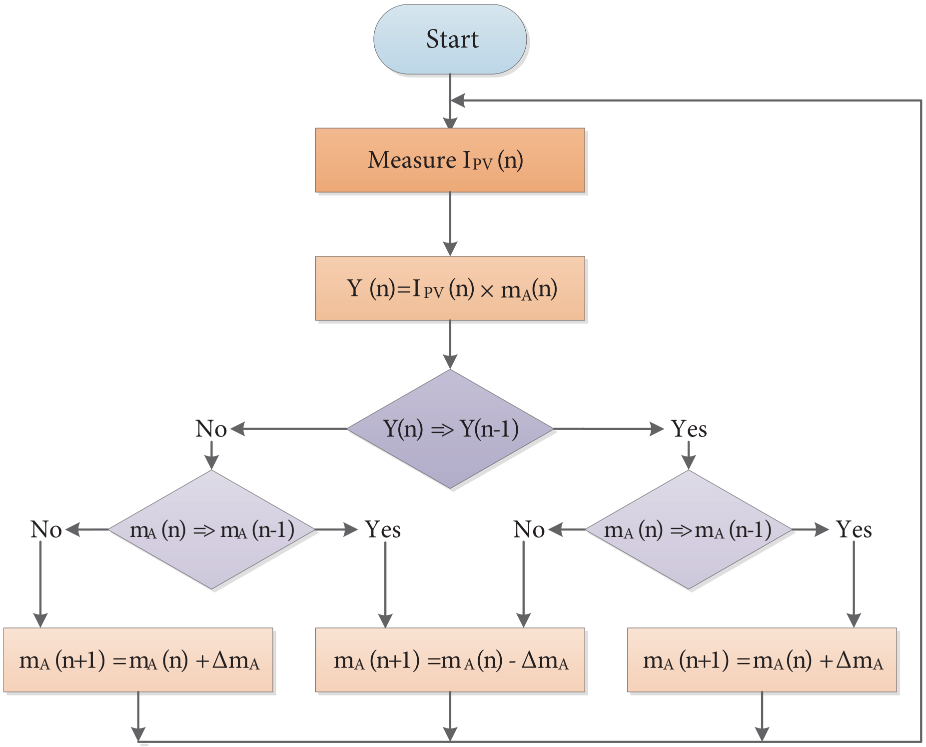

Figure 3. MPPT algorithm flow diagram using perturb-and-observe method.

In this study, the grid current is not measured directly but rather is estimated as the product of the modulation index and the measured solar cell output current as shown in Eq. (1):

$$I_{th} = \frac{m_A I_{CELL}}{\sqrt{2}}, \tag{1}$$

where I_{th} is the fundamental component of the unfolding circuit (H-bridge) output (grid) current and I_{CELL} is the PV array output current. The MPPT algorithm thus adjusts the modulation index to maximize the grid current magnitude.

2.2. Inverter simulation

The power electronic simulation package PSIM was used to simulate proposed current-source inverter, as seen in Figure 4, which shows the principal components of the inverter as well as the piecewise linear "4-diode" model that represents the PV array [16]. The 4-diode model allows fast and accurate simulations. The model is based on ideal zener diodes that have fixed voltage drops and it is fed by a constant-current source that is equal to I_{SC}. Additionally, the 4-diode model predicts the CSI input current ripple. Modeling of the oscillating input current is critical as this can cause substantial PV array output power losses as a result of the instantaneous deviations from the maximum power point. The semiconductor devices are also accurately modeled. The thyristor and reverse blocking diode voltage drops are taken into account and the on resistance of the MOSFET is included. Since the test setup included an autotransformer, the inductance and resistance of the autotransformer are also considered in the simulation model before the voltage source (grid).

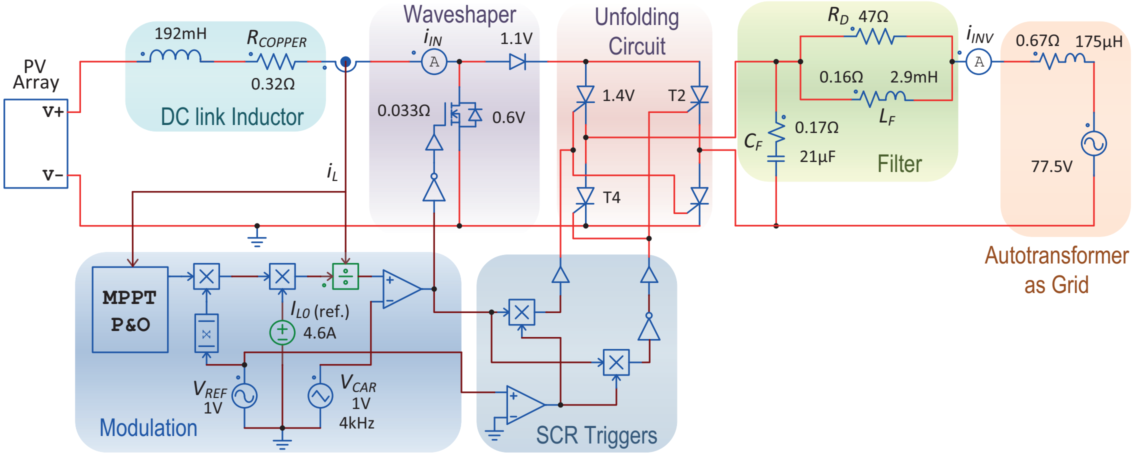

Figure 4. PSIM simulation of the proposed inverter, showing PV array (4-diode model), DC link inductor, waveshaper, unfolding circuit, output filter, grid model, MPPT controller, and PWM signal generator.

The feedforward control approach is introduced into the proposed converter by including the sensed PV array output current $i_L(t)$ and the desired WS output current I_{L0} amplitude to the open-loop control in Eq. (2). The relationship between the input and output current of the WS is seen in Eq. (3) for FFD control. Due to the PV array characteristic, the actual PV array current $i_L(t)$ is not equal to the nominal PV array output current I_{L0}. The algorithm to compensate the variations in $i_L(t)$ is shown in Eq. (3), which selects the appropriate duty cycle $d(t)$.

$$i_{OUT} = i_L[(1-d)m_A] \tag{2}$$

$$1 - d(t) = \frac{i^*_{IN}(t)}{i_L(t)} \quad \text{where} \quad i^*_{IN}(t) = I_{L0} m_A |\sin(\omega t)| \tag{3}$$

Here, $i^*_{IN}(t)$ represents the desired output current. Figure 4 shows the control circuit simulation model implementing the algorithm.

3. Experimental results

The CSI components, including the DC link inductor, waveshaper, output filter, and zero-crossing detection circuit, were optimized, built, and tested. Each stage will be explained below in depth.

Some of the component specifications of the proposed PV system are given in the Table. Figure 5 is also given to show the hardware implementation.

3.1. Energy storage inductor design

The aim of an energy storage inductor is to maintain a ripple free current in the DC link between the PV array and the inverter. There is a critical design trade-off for a PV grid-connected CSI regarding its energy storage inductor: increasing the amount of energy storage minimizes the PV array output power reduction but increases its size and cost. In addition, the DC link inductor has resistive losses and core losses that reduce the efficiency of the entire system. As a result, the optimization of the required value of DC link inductance is essential.

Table. Parameters of the 150 W current-source inverter.

Symbol	Parameter	Value
P_0	Rated maximum input power	164 W
V_{CELL}	Input voltage at P_0	35 V
I_0	Input current for P_0	4.55 A
P_{out}	Output power	142 W (avg)
V_{GRID}	Grid voltage	53.5 V (rms)
L_{DC}	DC link inductance	192 mH
E	DC link inductance energy storage	$\approx$ 12 mJ/W
R_{LDC}	DC link inductor resistance	0.32 Ω
L_F	Filter inductance	2.9 mH
C_F	Filter capacitance	21 μF
R_L	Filter inductance resistance	0.16 Ω
R_D	Filter damping resistance	47 Ω
R_{SW}	Waveshaper switch resistance	0.033 Ω
V_T	SCR voltage drop	1.3 V
V_D	Diode voltage drop	0.7 V
f_{sw}	PWM switching frequency	4 kHz

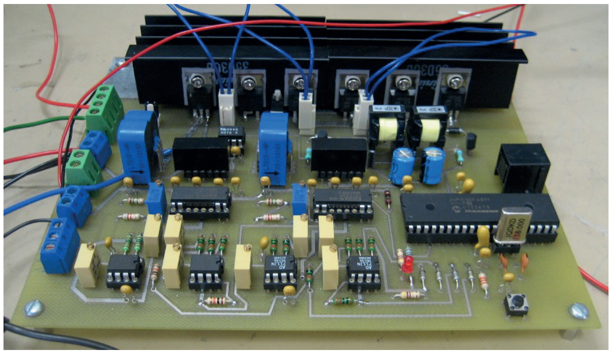

Figure 5. Photo of the CSI prototype showing the power electronics and control hardware.

Figure 6a shows a CAD drawing of the constructed inductor and Figure 6b shows the inductors for the 150 W grid-connected CSI based on the design calculations [21]. In this application, a 192 mH inductor with 0.34 Ω resistance has been used. The efficiency of the system was increased by the optimized inductor as the losses in the DC link inductor form a significant fraction of the total losses.

3.2. Current source inverter design

The basic aim of a current-source GCI is to feed a sinusoidal current into the power grid at unity power-factor, as seen in Figure 1. The constant current from the PV array and DC link inductor is chopped by the waveshaper (WS) switch employing a sinusoidal PWM control signal. A microcontroller (dsPIC30F4011) is used to create 4 kHz PWM signals using a sine function look-up table and the SCR H-bridge inverter is used to change the output current polarity to produce an AC output current. This is shown in Figure 7a, which shows the WS switch control signal and resulting circuit output current. Figure 7b shows both SCR pair pulses that unfold the WS current. A positive output current is obtained when T1 and T3 conduct and a negative output current when the T2–T4 pair conducts.

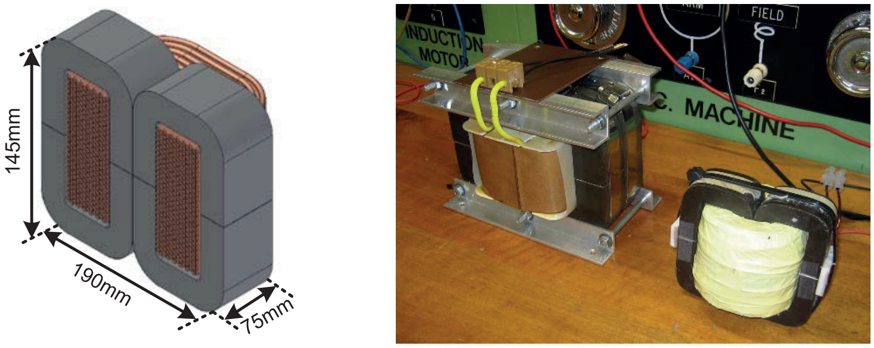

a) b)

Figure 6. a) CAD drawing of the energy storage inductor, which shows windings and C cores; b) constructed inductors.

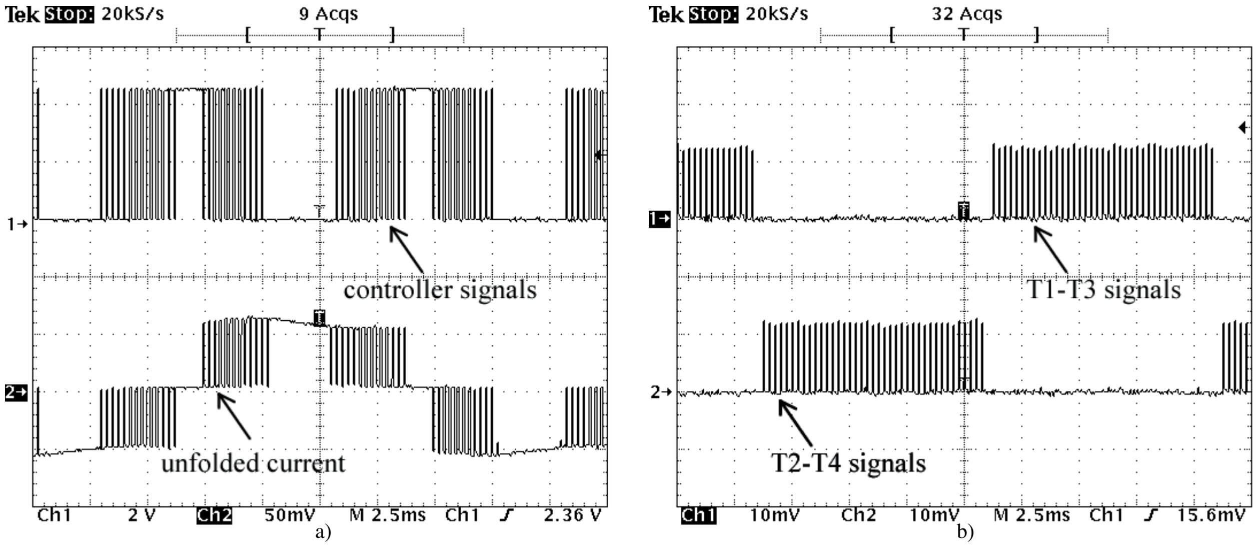

a) b)

Figure 7. Measured a) sinusoidal PWM signals from controller (top) unfolded output current (bottom), b) microcontroller output for SCR pair's drive pulses.

3.3. Low-pass filter design

The output low-pass filter reduces the high frequency harmonic content of the line current caused by the PWM switching. Generally the line filter consists of only a filter inductor (L filter) for VSIs but other configurations of inductors and capacitors such as CL filters for CSIs and LC and LCL filters for VSIs can be used.

It is well known that a GCI is required to provide high-quality power (low THD) to the grid while meeting the necessary power factor. The low-pass filter determines the harmonic attenuation and also affects the inverter power factor. However, the importance of the low-pass filter design is often overlooked. Such filters have copper and iron losses and hence reduce the overall inverter efficiency. The low-pass filter is designed such that the CSI is able to meet the following grid requirements [22] while exhibiting a low damping resistance (R_D) power loss (relative to rated power):

- a power factor between 0.8 lead and 0.95 lag, from 20% to rated output power, and,
- attenuating the high-frequency harmonics such that the output current contains less than 5% THD at rated output power.

For this application, a second-order CL-type low-pass filter is required as it allows the coupling of the current-source inverter to the voltage-source grid, according to the impedance mismatch criteria [23]. An example of this type of filter is shown in Figure 8.

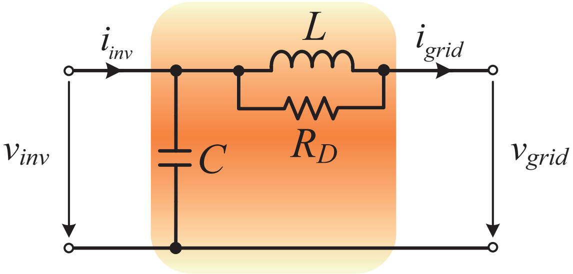

Figure 8. Parallel-damped CL type low-pass filter.

The filter cut-off frequency f_c is commonly referred to as the resonant frequency, f_R, as the filter has an infinite gain at that frequency if there is no damping resistance. The output filter must be carefully damped to limit any large amplifications at the resonant frequency. The resonant frequency can be given by:

$$f_R = \frac{1}{2\pi\sqrt{LC}} \tag{4}$$

The inverse of damping is quality factor Q, which is related to the gain of the filter at the resonant frequency. Note that the filter gain represents the ratio of output to input current, i.e. $I_{grid}/\ I_{inv}$ in Figure 8. The expression for Q is dependent on the filter topology and the type of damping used.

$$Q = \sqrt{\left(\frac{R_D}{Z_0}\right)^2 + 1} \quad \text{where} \quad Z_0 = \sqrt{\frac{L}{C}} \tag{5}$$

Above, Z_0 is the characteristic impedance of the filter. If the Q of the filter is too high an increase in THD can occur at the resonant frequency of the filter. If it is too low it will produce a large filter loss. The recommended values of Q for grid filters varies at 2–4 [23].

3.4. Grid synchronization

Grid synchronization is achieved using a simple mains voltage zero-crossing detector based on a comparator that compares the grid voltage to ground and generates a signal that is used to interrupt the microcontroller. The microcontroller uses this information to reset the SCR and WS look-up table duty cycle, hence outputting a current whose fundamental is synchronized to the grid (see Figure 9).

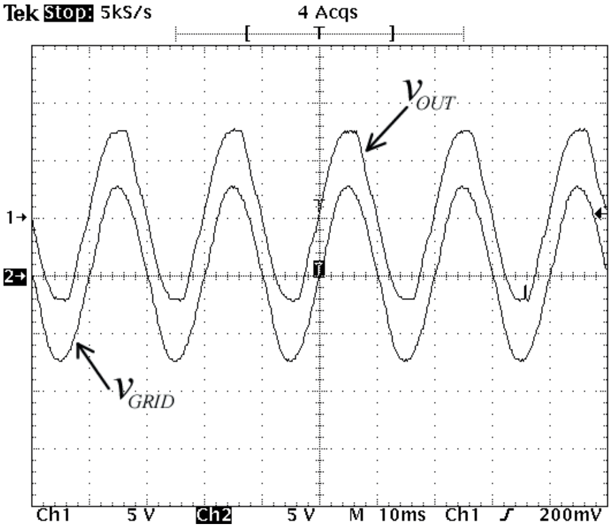

Figure 9. Synchronization of the output voltage of the inverter and the grid voltage. The vertical and horizontal scales are 50 V and 10 ms per division respectively.

The CSI output was connected to the mains through an isolated autotransformer to match the output voltage of the available PV array, and also for safety. The grid voltage via the autotransformer was set to 54 V rms. The autotransformer was modeled by an equivalent series inductor of 174 μH and series resistance of 0.67 Ω based on measurements.

3.5. Test procedure

The current-source GCI and the PV modules were tested in the laboratory. The PV modules were covered and the dark I-V method was used to simulate a solar irradiance of 1 kW/m^2. Preliminary experiments were done using a resistive load (21 Ω) after the low-pass filter. The inverter output current and voltage can be seen in Figure 10a.

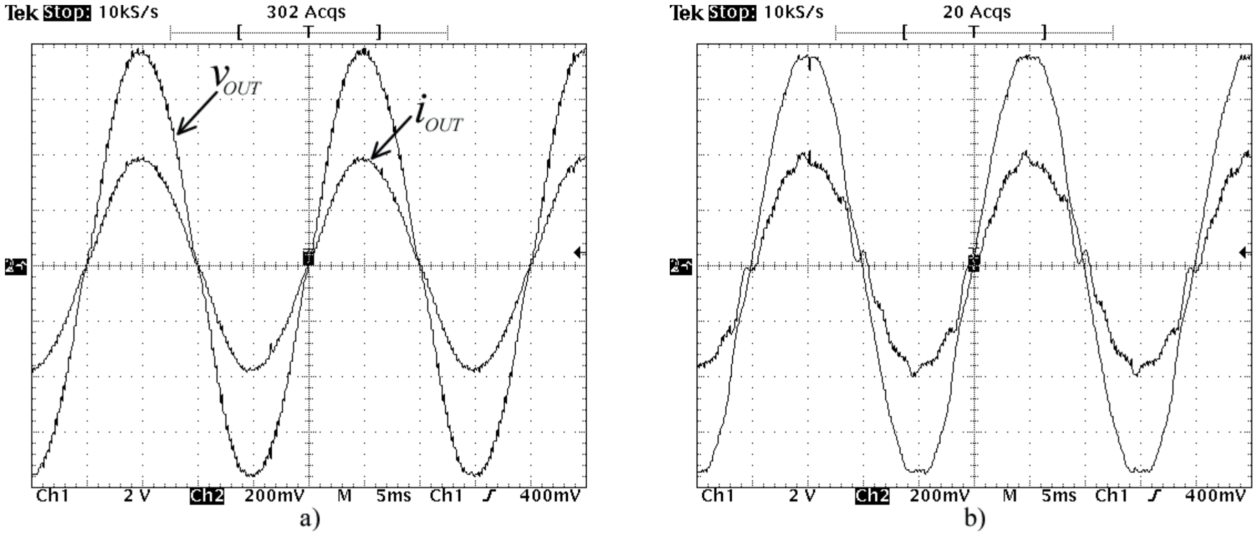

a)

b)

Figure 10. a) Inverter output current and voltage for resistive load case and b) for grid-connected case. The vertical and horizontal scales are 2 A, 20 V and 5 ms per division.

After the inverter output current and the grid voltage were synchronized the autotransformer output was connected in parallel with the resistive load and finally the resistive load was removed to achieve the grid-connected test case. This procedure for the grid synchronization is required to prevent large inrush currents. Figure 10b shows the inverter's voltage and current waveforms at the maximum operating power for the grid-connected case.

Figure 11 exhibits the simulated PV array output current and the grid-connected inverter output current at 85% m_A. The CSI output voltage is set to 54 V rms to be the same as the autotransformer voltage for synchronization. The control circuit phase advance was set to 13° in the simulation model to have good agreement. There is a substantial difference between the phase advance values used in the simulation model and the prototype (2.7°). This needs to be improved by fine-tuning the control algorithm as the CSI prototype requires the correct phase advance value for proper unfolding operation with the existing algorithm.

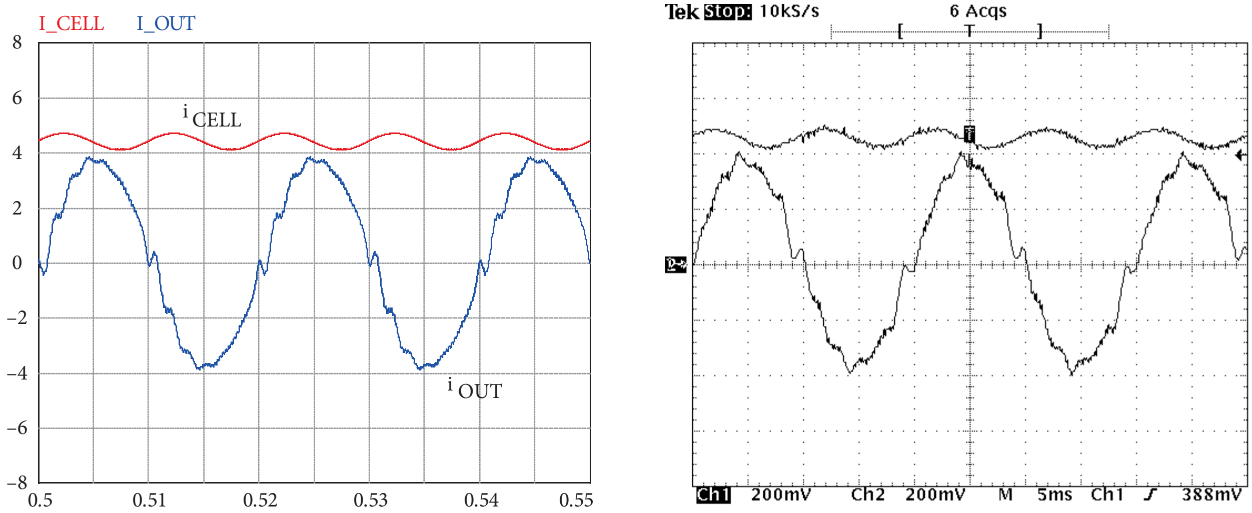

a)

b)

Figure 11. a) Simulated and b) measured CSI input and output currents for grid-connected case at 85% m_A. The vertical and horizontal scales are 2 A and 5 ms per division.

4. Performance analysis

The grid-connected CSI was tested to investigate its performance in the following areas:

- use of modulation index control to maximize the output power for a given irradiance condition,
- ability to meet the grid THD requirement of 5% at rated output power [22],
- ability to meet the grid power-factor requirements of 0.8 leading to 0.95 lagging from 20% to 100% of rated output power [22], and
- efficiency over the output power range.

During the tests, the dark I-V current source was set to standard irradiance conditions.

4.1. Modulation index and irradiance adjustments

Simulation and test results are shown in Figure 12a, where the output power is varied using the modulation index. P_0 corresponds to the maximum power point (MPP) where m_A is 0.85 and the power is maximum. The m_A of 85% is the optimum value for the CSI and this is shown in Figure 12a. The nominal m_A is chosen based on the trade-off between the ability for tracking the MPP under cold conditions versus the inverter efficiency. The measured results show good agreement with the simulations.

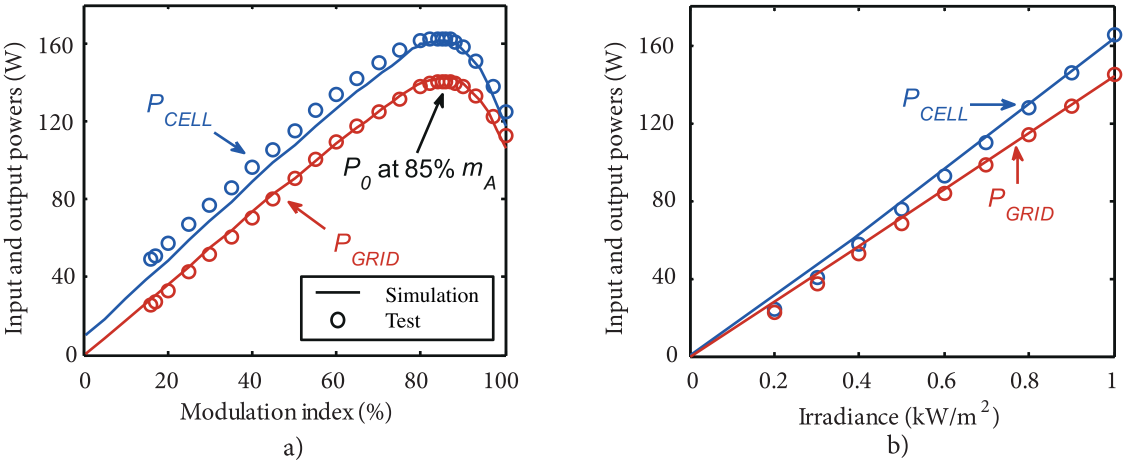

Figure 12. Simulated and measured CSI input (P_{CELL}) and output (P_{GRID}) powers for various a) modulation index and b) irradiance values (operating at MPP).

The input and output power versus irradiance curves are shown in Figure 12b. As mentioned in [21], the irradiance reduction causes an average power reduction as the PV array output current is directly proportional to irradiance, whereas the PV array output voltage is proportional to the modulation index while the current stays relatively constant due to the PV array I-V characteristics. Conduction losses are the major loss mechanism in the inverter and hence its losses increase with the PV array current. Due to the relatively constant current in the constant irradiation case in Figure 12a, the difference between the PV array output and the CSI output power remains almost constant.

However, in the changing irradiance case in Figure 12b, the power loss reduces proportional to the PV array output current, which results in higher efficiency at low output power levels.

4.2. Total harmonic distortion

The simulation and test results of the CSI output current THD by changing both the m_A and G values are shown in Figures 13a and 13b. Even though there is good correspondence in the THD at rated output conditions, there is significant error in the simulated results under light loads. This could be due to the switching losses in the power electronics devices and may be due to the phase advance angle modified to match with the rated output power test results. The phase angle value that is added to the simulation model is larger than the value used in the microcontroller. The required phase advance angle is directly proportional to the output power. Therefore, for light loads, a smaller phase advance is required. In addition, the large phase angle (13°) provides good correspondence with the rated output power but produces significantly larger THD than the test results for light loads.

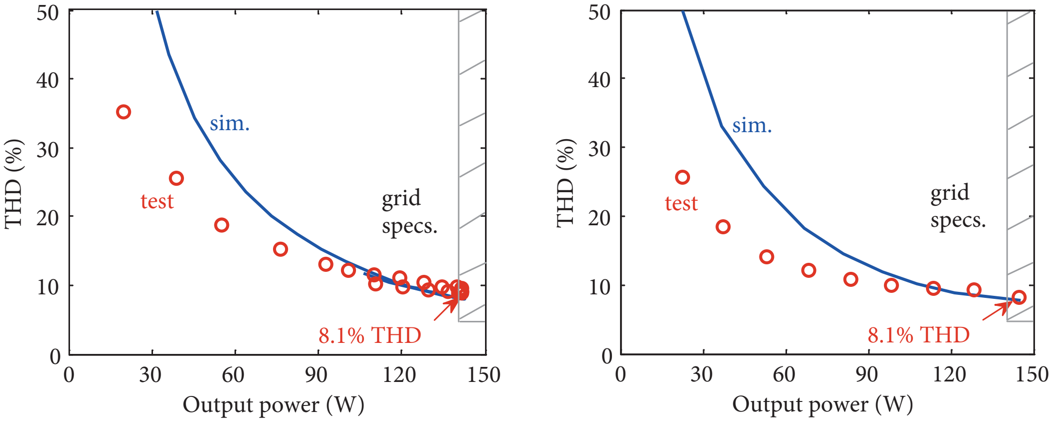

a) b)

Figure 13. Simulated and measured CSI THD as a function of output power for various a) modulation index and b) irradiance values (operating at MPP).

Likewise, in the changing irradiance case, the test results show good agreement with the simulations for the rated output power. In the test results, the output current THD for the G variations is lower than in the constant irradiance case in Figure 13b.

The measured grid-connected inverter current waveforms and their FFT spectra at nominal m_A are provided in Figure 14. Although they have high harmonic content there are slight differences between the current waveforms. Utilizing feedforward control reduces the THD by around 1%. The 3rd harmonic has a slight reduction and the 9th harmonic has a larger reduction than the open-loop case while the others remain relatively similar. These results imply that the output current distortion is not due to the 100-Hz PV array output current ripple. Possible causes include delays in the control algorithm implementation or phase shift in the grid filter causing issues with the unfolding circuit. Further investigation of means to improve this THD is required and this could include modifying the sinewave function look-up table.

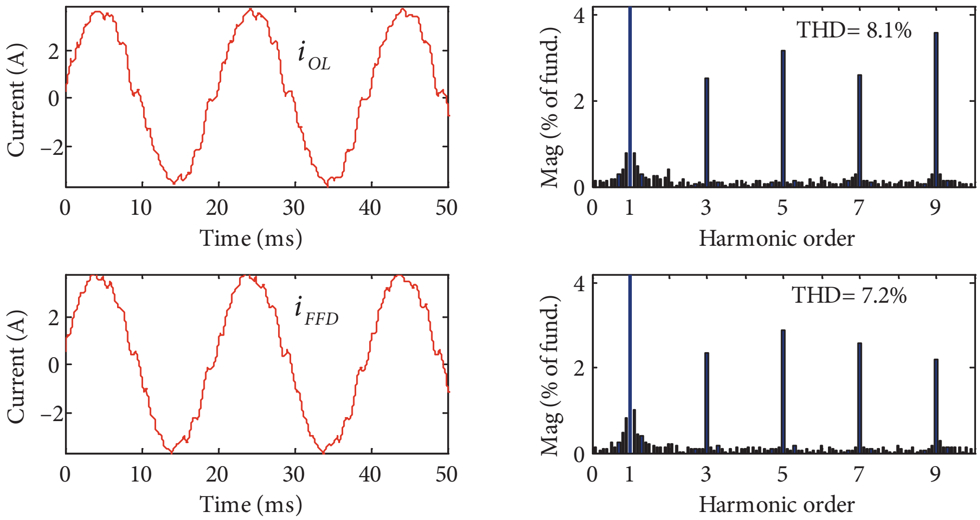

Figure 14. Measured output current waveforms of the CSI and their FFT spectra for open-loop (top) and feedforward (bottom) control cases.

4.3. Power factor

Figure 15a shows the simulated and measured results for the grid power factor as a function of modulation index. Note that during these studies the current was always leading, and the power factor is defined from the grid's point of view with regards to a passive load. The figure shows that the grid power factor requirement of at least 0.8 leading over the output power range of 20% to 100% of rated output has been met.

Figure 15b illustrates power factor curves for the varying irradiance conditions and, similar to the modulation index variations, the grid specification of the power factor is achieved. As the inverter operates at the MPP for each irradiance case, the PF for light loads is slightly better for the varying irradiance case in Figure 15b.

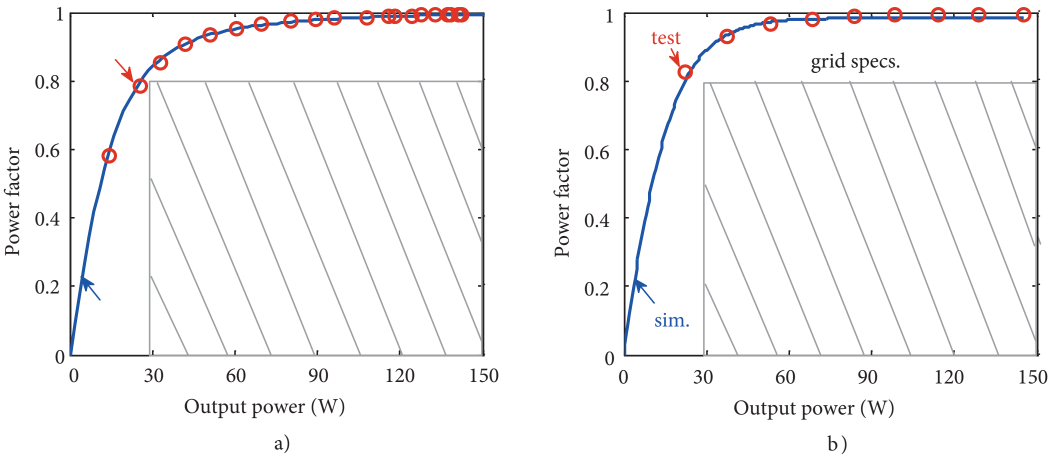

Figure 15. Simulated and measured CSI power factor as a function of output power for various a) modulation index and b) irradiance values (operating at MPP).

4.4. Efficiency

The inverter efficiency can be measured using the input power P_{CELL} and the output power P_{GRID}. The efficiency measurement was performed using a power analyzer (Voltech-PM3000A). Even though there is good correspondence in the efficiency at rated output conditions, there is significant error in the simulated results under light loads for the initial test results (see Figure 16a). The error may be due to the wiring between the inverter and the external measuring devices, such as the power analyzer. Although the cables used are capable of carrying the maximum current (4.8 A), they have significant copper losses. In a second test, the thickness of the cables was increased, which resulted in higher efficiency and simulation results now show good agreement with the measured results.

Figure 16b illustrates the efficiency as a function of output power at the MPP for each irradiance value. The resultant efficiency curve is different than that obtained by changing m_A with constant irradiance as the PV array output current is proportional to irradiance. This results in lower resistive losses and hence higher efficiency.

5. Conclusions

This paper examined the implementation and performance evaluation of a low-cost 150 W single-phase current-source grid-connected PV inverter.

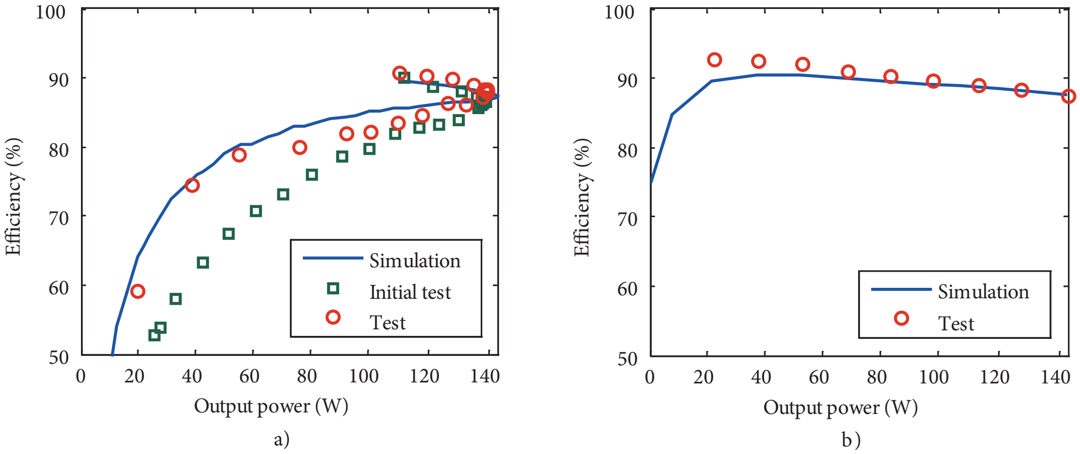

Figure 16. Simulated and measured CSI efficiency as a function of output power for various a) modulation index b) irradiance values.

It was shown that the CSI could meet the grid power factor requirement over the required 20% to 100% of output power but that the inverter THD of 8.1% at rated output power did not meet the 5% requirement due to low frequency current harmonics. The feedforward control implementation improved the inverter output current waveform only slightly. These current harmonics are likely due to unwanted delays in the system [24] or phase shift in the grid filter causing issues with the unfolding circuit. Further investigation of means to improve this THD is required and this could include modifying the sinewave function look-up table.

The efficiency of the inverter was examined over a range of output powers for modulation index and irradiance variations. The calculated results showed good agreement with the measurements at rated output power. However, the measured efficiency at light load was lower than the predictions, likely caused by the unmodeled semiconductor switching and external cabling losses.

References

[1] McMurray W. The performance of a single-phase current-fed inverter with counter emf-inductive load. IEEE T Ind Appl 1978; 14: 319–329.

[2] Neba Y, Furuyama E. Calculation of maximum power in a utility-interactive photovoltaic-generating system by using PWM current-source inverter. Electr Eng Jpn 1998; 125: 55–64.

[3] Hirachi K, Matsumoto K, Yamamoto M, Nakaoka M. Improved control implementation of single-phase current-fed PWM inverter for photovoltaic power generation. In: IEE 1998 International Conference on Power Electronics and Variable Speed Drives; 21–23 September 1998; London, UK. London, UK: IEE. pp. 63–68.

[4] Nonaka S, Kesamaru K, Yamasaki K, Nishi M. Interconnection system with single phase IGBT PWM CSI between photovoltaic arrays and the utility line. In: IEEE 1990 Industry Applications Society Meeting; 7–12 October 1990; Seattle, WA, USA. New York, NY, USA: IEEE. pp. 1302–1307.

[5] Itoh R, Ishizaka K, Oishi H, Okada H. Soft-switched current-source inverter for single-phase utility interfaces. Electron Lett 2001; 37: 1208–1209.

[6] Han BM, Kim HJ, Baek ST. New soft-switching current source converter for photovoltaic power system. Electr Eng 2004; 86: 285–229.

[7] Wu B. High Power Converters and AC Drives. 1st ed. New York, NY, USA: Wiley-IEEE Press, 2006.

[8] Chen M, Lee X, Tsutomu Y. A novel soft-switching grid-connected PV inverter and its implementation. In: IEEE 2011 Power Electronics and Drive Systems Conference; 5–8 December 2011; Singapore. New York, NY, USA: IEEE. pp. 373–378.

[9] Kyritsis AC, Tatakis EC, Papanikolaou NP. Optimum design of the current-source flyback inverter for decentralized grid-connected photovoltaic systems. IEEE T Energy Conver 2008; 23: 281–293.

[10] Bush CR, Wang B. A single-phase current source solar inverter with reduced-size DC link. In: IEEE 2009 Energy Conversion Congress and Exposition; 20–24 September 2009; San Jose, CA, USA. New York, NY, USA: IEEE. pp. 54–59.

[11] Tofoli FL, Schonell JC, Gallo CA, Sanhueza SMR. A low cost single-phase grid-connected photovoltaic system with reduced complexity. In: IEEE 2009 Power Electronics Conference, 27 September–1 October 2009; Bonito-Mato Grosso do Sul, Brazil. New York, NY, USA: IEEE. pp. 1033–1038.

[12] Nousiainen L, Suntio T. Dynamic characteristics of current-fed semi-quadratic buck-boost converter in photovoltaic applications. In: IEEE 2011 Energy Conversion Congress and Exposition; 17–22 September 2011; Phoenix, AZ, USA. New York, NY, USA: IEEE. pp. 1031–1038.

[13] Roman IT, Silva LS. A single-phase current-source inverter with active power filter for grid-tied PV systems. In: IEEE 2012 Power Electronics for Distributed Generation Systems; 25–28 Jun 2012; Aalborg, Denmark. New York, NY, USA: IEEE. pp. 349–356.

[14] Ohnuma Y, Orikawa K, Itoh JI. A single-phase current source PV inverter with power decoupling capability using an active buffer. IEEE T Ind Appl 2015; 51: 531–538.

[15] Whaley DM, Ertasgin G, Soong WL, Ertugrul N, Darbyshire J, Dehbonei H, Nayar CV. Investigation of a low-cost grid-connected inverter for small-scale wind turbines based on a constant-current source pm generator. In: IEEE 2006 Industrial Electronics Society Conference; 6–10 November 2006; Paris, France. New York, NY, USA: IEEE. pp. 4297–4302.

[16] Ertasgin G, Whaley DM, Ertugrul N, Soong WL. A current-source grid-connected converter topology for photovoltaic systems. In: The Australasian Universities Power Engineering Conference; 10–13 December 2006; Melbourne, Australia.

[17] Ertasgin G, Whaley DM, Ertugrul N, Soong WL. Implementation and performance evaluation of a low-cost current-source grid-connected inverter for PV applications. In: IEEE 2008 Sustainable Energy Technologies Conference; 24–27 November 2008; Singapore. New York, NY, USA: IEEE. pp. 939–944.

[18] Ertasgin G, Soong WL, Ertugrul N. Analysis and design of single-phase current-source grid-connected PV inverter. In: IEEE 2013 Power Electronics and Applications Conference; 2–6 September 2013; Lille, France. New York, NY, USA: IEEE. pp. 1–10.

[19] Soong WL, Ertugrul N. Inverterless high power interior permanent magnet automotive alternator. IEEE T Ind Appl 2004; 40: 1083–1091.

[20] King DL, Hansen BR, Kratochvil JA, Quintana MA. Dark current-voltage measurements on photovoltaic modules as a diagnostic or manufacturing tool. In: IEEE 1997 Photovoltaic Specialists Conference; 29 September–3 October 1997; Anaheim, CA, USA. New York, NY, USA: IEEE. pp. 1125–1128.

[21] Ertasgin G, Whaley DM, Ertugrul N, Soong WL. Analysis and design of energy storage for current-source 1-ph grid-connected PV inverters. In: IEEE 2008 Applied Power Electronics Conference and Exposition; 24–28 February 2008; Austin, TX, USA. New York, NY, USA: IEEE. pp. 1229–1234.

[22] Standards Australia. Grid Connection of Energy Systems via Inverters, Standards Australia, Australian Standards Documents, Sections AS 4777.1, AS 4777.2, AS 4777.3. Sydney, Australia: Standards Australia, 2005.

[23] Nave MJ. Power Line Filter Design for Switched-Mode Power Supplies. New York, NY, USA: Van Nostrand Reinhold, 1991.

[24] Abeyasekera T, Johnson CM, Atkinson DJ, Armstrong M. Elimination of subharmonics in direct look-up table (DLT) sine wave reference generators for low-cost microprocessor-controlled inverters. IEEE T Power Electr 2003; 18: 1315–1321.